Exfoliation of metal-organic framework nanosheets using surface acoustic waves

Xia Liu [a],[b], Qinxiang Jia [c], Yongqing Fu [d], Tengfei Zheng [a],[b],[*]

[a] State Key Laboratory for Manufacturing Systems Engineering Xi'an Jiaotong University, Xi'an 710049, People's Republic of China
[b] Shaanxi Key Lab of Intelligent Robots, Xi'an Jiaotong University, Xi'an 710049, People's Republic of China
[c] Department of Chemistry, Xi'an Key Laboratory of Sustainable Energy Materials Chemistry, Xi'an Jiaotong University, Xi'an 710049, People's Republic of China
[d] Faculty of Engineering & Environment, Northumbria University, Newcastle upon Tyne NE1 8ST, UK

ARTICLE INFO

ABSTRACT

Two-dimensional (2D) metal–organic framework (MOF) nanosheets have recently received extensive attention due to their ultra-thin thickness, large specific surface area, chemical and functional designability. In this study, an unconventional method using surface acoustic wave (SAW) technology is proposed to exfoliate large quantities and uniform layers of 2D MOF-$Zn_2(bim)_4$ nanosheets in a microfluidic system. We successfully demonstrated that the thickness of 2D MOF is effectively and accurately controlled by optimizing the SAW parameters. The mechanisms for the efficient exfoliation of 2D MOF nanosheets is attributed to both the electric and acoustic fields generated by the SAWs in the liquid. The electric field ionizes the methanol to produce H^+ ions, which intercalate $Zn_2(bim)_4$ sheets and weaken the interlayer bonding, and the strong shear force generated by SAWs separates the MOF sheets. A yield of 66% for monolayer MOFs with a maximum size of 3.5 μm is achieved under the combined effect of electric and acoustic fields. This fast, low-energy exfoliation platform has the potential to provide a simple and scalable microfluidic exfoliation method for production of large-area and quantities of 2D MOFs.

1. Introduction

Compared with three-dimensional (3D) bulk nanomaterials, two-dimensional (2D) nanosheets, such as those based on graphene[1,2], black phosphorus[3], transition metal dichalcogenide[4], transition metal carbides and nitrides (MXenes)[5], and metal organic frameworks (MOF)[6], have many advantages due to their intrinsic ultrathin structures, excellent mechanical flexibility, good optical transparency, large specific surface area, and abundant catalytic active sites[7]. Among them, 2D MOF nanosheets with their excellent mechanical flexibility[8], adjustable pore size, and chemical and functional designability[9], have shown great potentials for applications in sensing[10,11], electronics [12,13], energy[14], gas separation[15], and biocatalysts[16].

The commonly used preparation methods for 2D MOF nanosheets are mainly divided into two categories, i.e., bottom-up and top-down. Bottom-up approaches such as interfacial synthesis[17,18], surfactant-assisted synthesis[19–21], three-layer modulated synthesis[22], directly achieve the synthesis of 2D MOF nanosheets through metal-containing organic linkers. However, they have disadvantages. For examples, the obtained nanosheets have a thick layer and the surfactant often strongly adheres to the nanosheet surfaces[21,22]. These defects hinder the exposure of more active sites, and cause major problems for the application of 2D MOFs. The top-down methods, including ultra-sonication[23,24], ball milling[25] and shear mixing[26], are effective in obtaining high yield suspensions of 2D MOF flakes[27]. They mostly rely on the external forces to agitate fluid with high speeds, thus resulting in strong shear forces in the fluid to exfoliate the MOFs. The processing time is varied from ten of minutes to a few hours [24,26,28,29]. However, the thickness distribution is often not uniform, ranging from a few nanometers to hundreds of nanometers[24,29]. They also have drawbacks including high energy consumption, inability to obtain high yields of monolayer nanomaterials, and difficulty in production of large-scale single layer sheets. Therefore, there is an urgent need to find other types of simple but efficient methods to obtain nanosheets with a monolayer thickness in a large scale.

Surface acoustic waves (SAWs) are electromechanical waves with nanometers or sub-nanometer amplitudes propagating along the surface of a piezoelectric substrate, accompanied by changes in the electric field
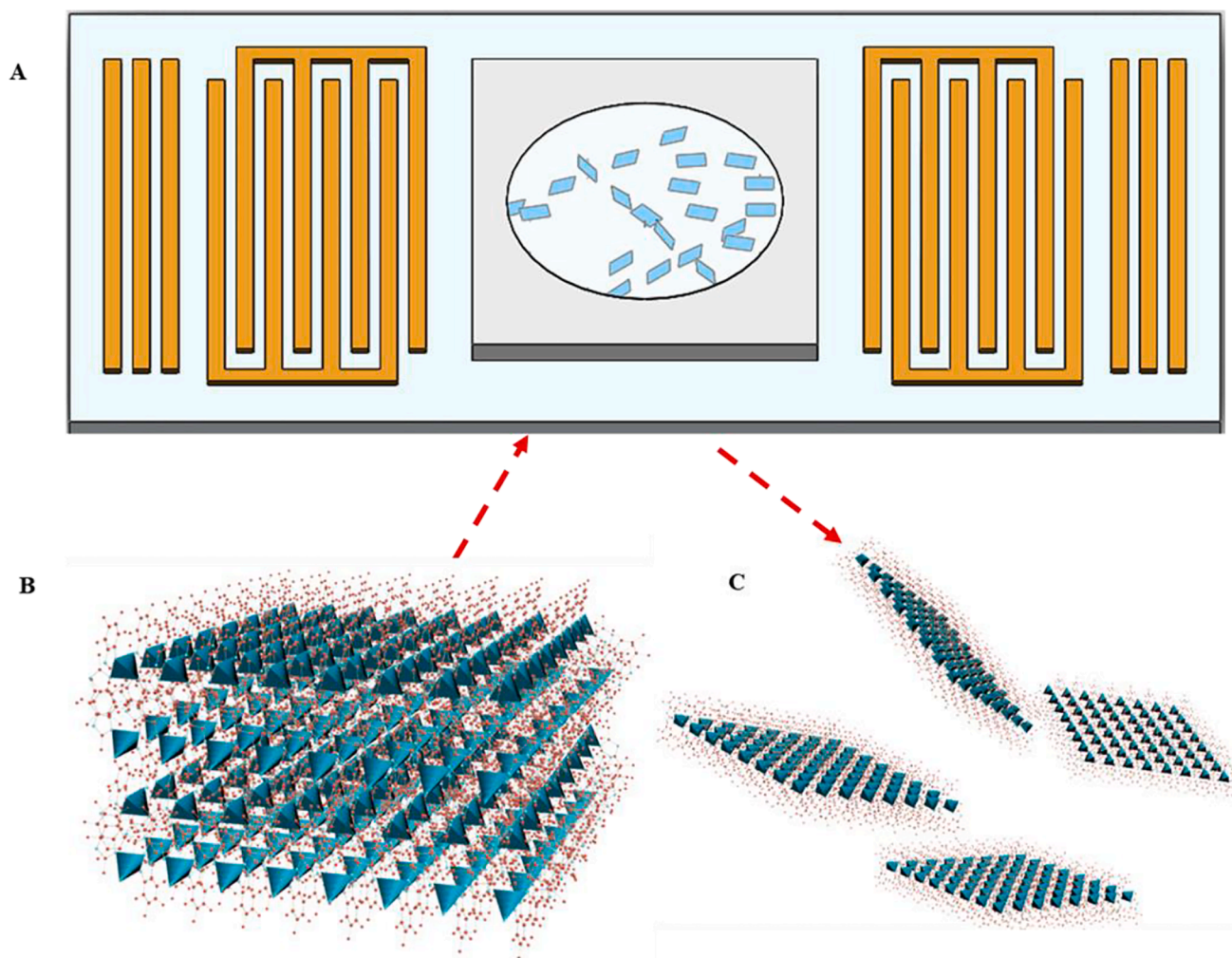

Fig. 1. Illustrations of SAW exfoliation device and $Zn_2(bim)_4$ structures. (A) Illustration of the SAW exfoliation device constituting an LN chip with a PDMS reservoir bonded onto it. (B) Illustration of bulk $Zn_2(bim)_4$ structure. (C) Illustration of monolayer $Zn_2(bim)_4$ nanosheets structure.

along its propagation path. The wave energy is concentrated within one wavelength depth of the device surface, and the wave energy is dissipated into the liquid, which forms an efficient method for driving liquids at the microscale level [30,31]. The large shear force generated in the liquid can effectively exfoliate the bulk materials into 2D nanosheets [5,32,33]. SAWs have many advantages over the conventional ultrasonic waves, including simple operation, low power consumption, and easy control of acoustic energy[34]. They have advantages to control the thickness of the exfoliated 2D nanosheets due to its combination of strong acoustic and electric fields within the liquid. For example, Mohiuddin et. al [32] reported that the electric field generated by the propagating SAWs plays a dominant role in exfoliating MoS_2 for ultra-thin layers with a large dimensional size. Yang et. al[35,36] reported that electrochemistry has a significant impact on exfoliation of 2D MOF. However, it is not fully understood how the different and separate effects of electric field and acoustic field generated by the SAWs within the liquid on the exfoliation principles of 2D materials.

In this paper, we use the SAW exfoliation method to prepare MOF-$Zn_2(bim)_4$ (bim = benzimidazole) nanosheets, from bulk $Zn_2(bim)_4$ materials. The obtained 2D MOF structure is highly stable and microcrystalline after exfoliation[37,38]. 2D $Zn_2(bim)_4$ nanosheets have a variety of applications, such as membranes for separation and purification of hydrogen gas from CO_2 [39], purification of water[37], and laser desorption/ionization of small molecules[28]. We find that the thickness of the obtained nanosheets can be easily controlled by regulating the SAW durations and we obtain single layer nanosheets with

sizes up to 3.5 μm. Most importantly, we verify that the accompanying electric field generated by the SAW effectively facilitate the exfoliation process of 2D $Zn_2(bim)_4$. In combination of joint influences of acoustic wave and electric field generated by SAWs, large-area, uniformly distributed ultrathin 2D $Zn_2(bim)_4$ nanosheets have been obtained.

2. Experiment section

2.1. Fabrication of SAW device

A 4-inch single crystalline $LiNbO_3$ (LN, 128° Y-rotated X-cut, 1 mm thick) wafer was used as the substrate. Interdigital transducers (IDTs, 20 pairs) with their reflectors were patterned on the LN wafer, with a 20 nm chromium adhesive layer and a 80 nm gold layer[40]. The IDTs have a wavelength of 400 μm (corresponding to the resonance frequency of 9.7 MHz) and its reflector of 100 μm width. The resonant frequency of the device was characterized using a vector network analyzer (N5232A). A signal generator (AFG3022, USA) and an amplifier (TREK MODEL 2100HF) were used to apply RF signals to the SAW IDTs at its resonance frequency of ∼ 9.7 MHz for the acoustofluidic tests.

2.2. Preparation of PDMS liquid reaction reservoir

PDMS curing agent was mixed with the prepolymer at a mass ratio of 1:10. The mixture was ultrasonically stirred for 5 min, and then the air bubbles were removed by keeping it in a vacuum chamber. The prepared
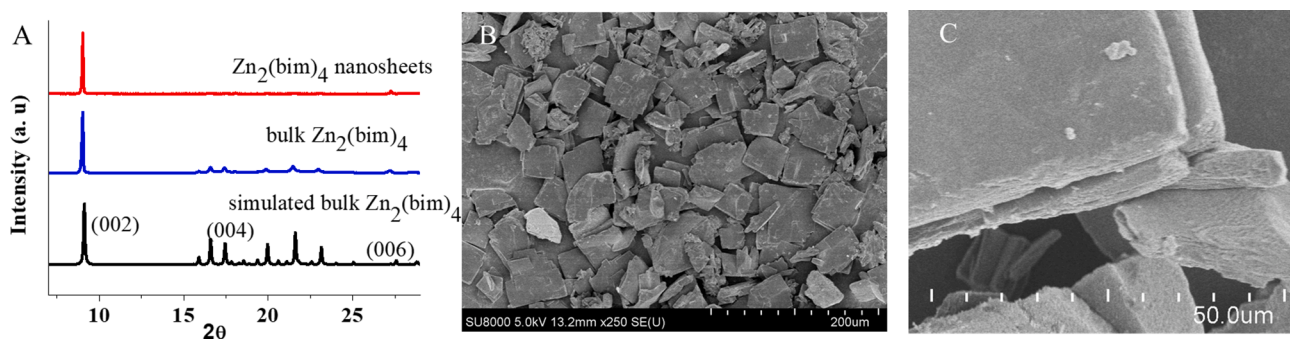
Fig. 2. Characterization of bulk $Zn_2(bim)_4$. (A) The XRD patterns of bulk $Zn_2(bim)_4$ and $Zn_2(bim)_4$ nanosheets. (B) The SEM image of the bulk $Zn_2(bim)_4$ materials. (C) The typical layered structure morphology of $Zn_2(bim)_4$.

PDMS solution was poured into a plastic Petri dish to form a layer of 2 mm thick and cured in an oven. The curing temperature was 80 °C for 1 h. After curing, the PDMS chamber was prepared by punching a hole with a diameter of 9 mm for microchamber connection. The PDMS chamber and the LN wafer with IDTs were then placed inside a plasma chamber and treated with plasma. Then the treated PDMS layer was pressed onto the LN layer for bonding, and the bonded device was placed in an oven at 110 °C for 1 h, before cooling down to room temperature [41]. The fabricated SAW device for exfoliation is shown in Figure S4.

2.3. Preparation of bulk $Zn_2(bim)_4$

Bulk $Zn_2(bim)_4$ precursors were prepared based on the hydrothermal transformation of ZIF-7 nanoparticles[25]. Firstly, 0.605 g of zinc nitrate hydrate ($Zn(NO_3) \cdot 6H_2O$, 99.99%) and 1.539 g of benzimidazole (bim, >98%) were added in 200 mL of N,N-dimethylformamide (DMF, AR). After stirring for 1 h, the mixed solution was left for 72 h at room temperature. The formed ZIF-7 nanoparticles were collected by centrifugation and washed with methanol. The collected sediment was dried at 50 °C for 12 h, followed by drying in a vacuum oven at 120 °C for 48 h. Next, 0.34 g dried ZIF-7 nanoparticles were dispersed in deionized (DI) water up to a concentration of 0.5 wt% and then heated at 100 °C for 24 h. Finally, the $Zn_2(bim)_4$ was obtained by centrifugation and washed with DI water and methanol. The collected sediment was dried at 50 °C overnight.

2.4. Nanosheet preparation

$Zn_2(bim)_4$ powder of 2.5 mg was added into 10 mL MeOH/n-propanol mixture (V: V = 1: 1). In the exfoliation process, the above liquid mixture with a volume of 120 μL was put into the PDMS reservoir. The operating frequency of the SAWs device was 9.7 MHz and the applied voltage was 15 V. The SAW agitation durations varied from 1, 10, 20, 60 and 90 min. After the exfoliation, the liquid in the PDMS chamber was transferred into a 1.5 mL centrifuge tube and diluted to 1 mL solution with a mixture of MeOH/n-propanol. The supernatant was collected for characterization after it was centrifugated at 9000 rpm for 25 min. The collected supernatant was dropped into the PDMS chamber on the SAW device and dried in a vacuum oven until the supernatant was changed into white $Zn_2(bim)_4$ nanosheet powder.

2.5. Characterization

Crystalline structures of both the prepared $Zn_2(bim)_4$ bulk and $Zn_2(bim)_4$ nanosheets were characterized using X-ray diffraction (XRD, D8 ADVANCE A25, Germany). Morphology of $Zn_2(bim)_4$ bulk was characterized using a scanning electron microscope (SEM, SU8000, Japan). $Zn_2(bim)_4$ nanosheet suspensions were added onto a copper-supported ultrathin carbon grid (200 mesh, Chukyo Kiyo Co.), for characterization using a transmission electron microscope (TEM, JEOL

JEM-F200) and a high-resolution TEM (HRTEM, JEOL JEM-2100Plus) with the attached energy dispersive X-ray spectroscope (EDX). The $Zn_2(bim)_4$ nanosheet suspension was dropped onto the silicon substrate (1 cm × 1 cm), and then dried in a vacuum oven to characterize the surface topography and thickness profile using an atomic force microscope (AFM, Bruker Dimension Icon, INNOVA). At least 50 particles per experimental condition were tested during the AFM analysis and the average readings were obtained.

3. Results and discussion

Fig. 1 shows the exfoliation device, including a lithium niobate ($LiNbO_3$, LN) wafer and a polydimethylsiloxane (PDMS) chamber. The illustrations of $Zn_2(bim)_4$ structure before and after the exfoliation processes are represented in Fig. 1B and 1C, respectively.

Fig. 2A shows the XRD pattern of bulk $Zn_2(bim)_4$, which is matched with the reference of (CCDC-675375)[25], proving that the $Zn_2(bim)_4$ was successfully synthesized. Fig. 2B shows an SEM image of the bulk $Zn_2(bim)_4$, showing numerous block structures. Fig. 2C shows an SEM image of the typical layered structure of the $Zn_2(bim)_4$.

The bulk $Zn_2(bim)_4$ material was exfoliated by the SAWs device as shown in Figure S5. Fig. 3 shows the AFM images of $Zn_2(bim)_4$ nanosheets obtained from samples with SAW exposure durations from 1 to 90 min, along with their thickness distribution histograms. Fig. 3A shows a large thickness distribution in the range 6–27 nm ($M = 17$ nm, M represents the median thickness of 50 nanosheets) for the sample exposed to SAWs for 1 min. With increasing the exposure time, the thicknesses of nanoflakes gradually decreased as shown in Fig. 3A to 3E. At an exposure time of 20 min (Fig. 3C), the thickness of nanosheets was 5 nm (e.g., ~5 layers with a single layer thickness of ~ 0.98[25]). The SAW exfoliated sample for 20 min was analyzed by XRD, and the result is shown in Fig. 2. It matches well with that of the bulk $Zn_2(bim)_4$, which demonstrates that the exfoliation process did not destroy the crystalline structure of $Zn_2(bim)_4$. When the SAW exposure time increased to 90 min, almost 90% of the nanosheets samples was less than 3-layer thick as shown in Fig. 3E. The estimated yield of monolayers obtained is 66%, which is the percentage of monolayer nanosheets obtained from 50 nanosheets.

Fig. 4 shows TEM and HRTEM images of $Zn_2(bim)_4$ nanosheets exposed to SAWs for 20 min and 90 min, respectively, along with the energy dispersive X-ray (EDX) mapping patterns of elements. The Tyndall effect of $Zn_2(bim)_4$ nanosheet solution (the inset in Fig. 4A) was observed which confirms that they are colloidal materials[42]. TEM images of the obtained $Zn_2(bim)_4$ nanosheets (Fig. 4A and 4B) show wrinkle patterns, which indicate the flexibility of the obtained nanosheets[43]. The HRTEM (the inset in Fig. 4B) image shows that the fringe spacing of the $Zn_2(bim)_4$ nanosheets is ~0.34 nm, corresponding to the (0 0 6) lattice plane of the $Zn_2(bim)_4$ with a lattice constant of ~ 0.32 nm[25]. Fig. 4C and 4D show that the monolayer materials have been obtained when the exposure time is 90 min. The EDX elemental
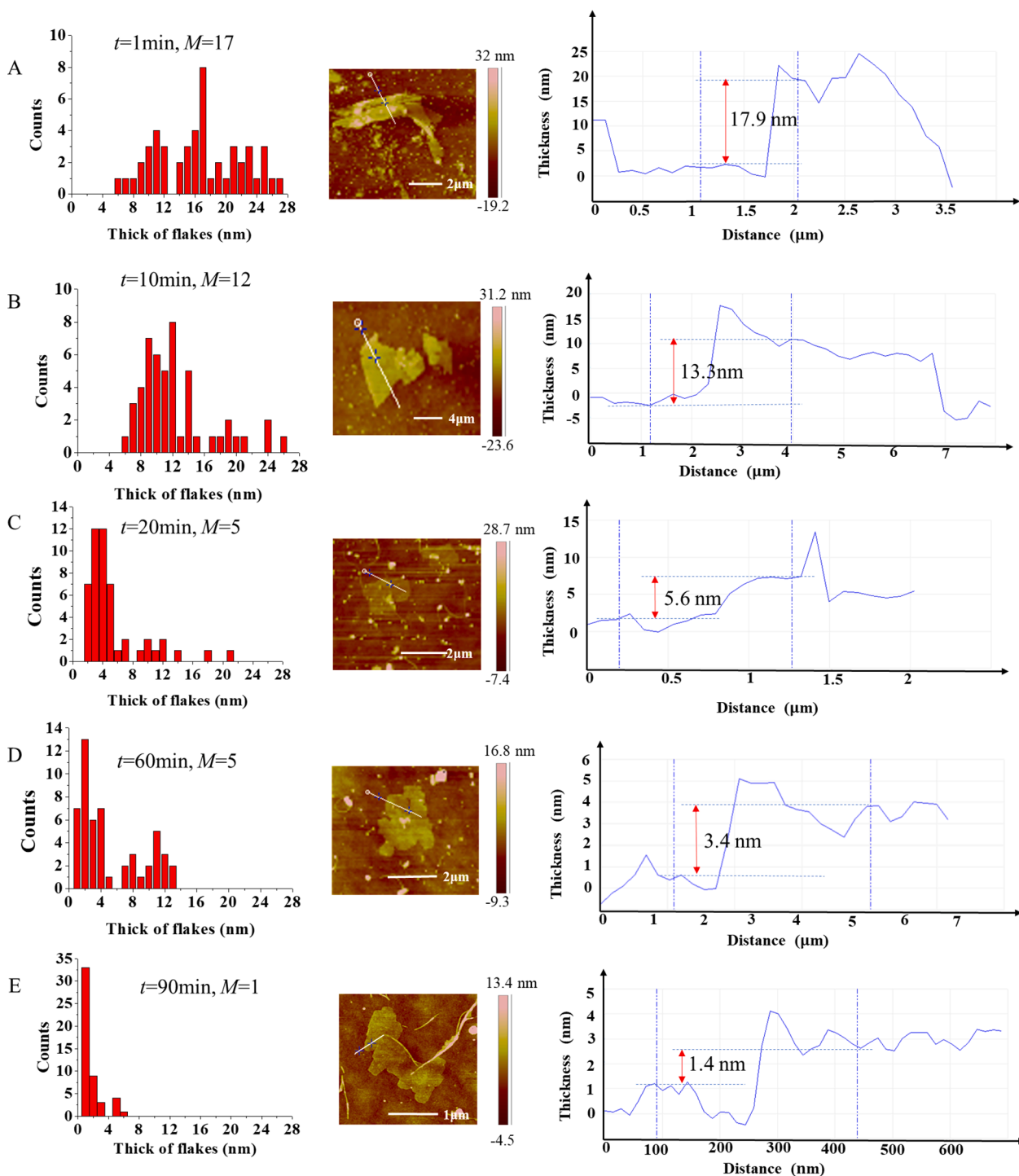
Fig. 3. Thickness distribution of $Zn_2(bim)_4$ nanoflakes obtained from the AFM measurements. Thickness distribution histograms of the exfoliated $Zn_2(bim)_4$ nanoflakes, along with typical images and height profile at different SAW exposure durations of (A) 1 min, (B) 10 min, (C) 20 min, (D) 60 min and (E) 90 min. t represents the exposure time and M represents the median thickness of 50 nanosheets.

mapping images in Fig. 4E show that C, N, O and Zn are distributed uniformly inside the nanosheets[26,44,45].

To investigate the effect of electric field generated by the SAWs on exfoliation of the MOFs, we have made two additional microchips for exfoliation, which are different from the SAW chip (as shown in Figure S7 (A)).

The first one (Figure S7 (B)) only produces an acoustic wave field, by depositing a metal (20 nm thick Cr adhesive and 80 nm thick Au) layer between the PDMS chamber and the LN substrate. The metal layer

between the LN substrate and PDMS can shield the electric field after the voltage is applied. The second one (Figure S7 (C)) can only generate an electric field with the IDTs patterned on glass substrate (without any piezoelectric material) and the PDMS chamber pressed onto the IDTs position. The obtained current–voltage (*I-V*) curves are shown in Fig. 5A, which reveals the currents in methanol/n-propanol mixture on three different chips. The electrolytic current becomes much larger when the SAW driving voltage is increased from 0 V to 15 V. This is mainly due to generation of more H^+ ions from the ionization of methanol, when the
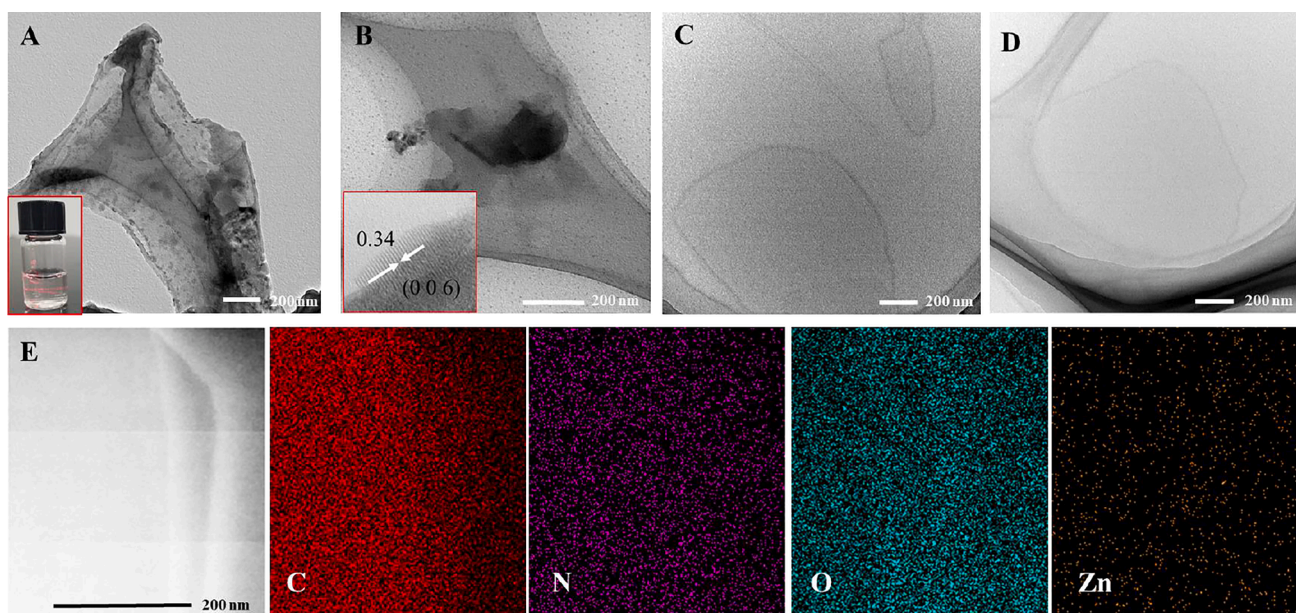
Fig. 4. TEM image of a piece of $Zn_2(bim)_4$ nanosheets. TEM images of the $Zn_2(bim)_4$ nanoflakes for different SAW exposure durations: (A) 20 min samples with tyndall effect image of $Zn_2(bim)_4$ nanosheets, (B) 20 min samples with a HRTEM image, (C) and (D) 90 min samples. (E) The EDX mapping image of $Zn_2(bim)_4$ nanosheet.
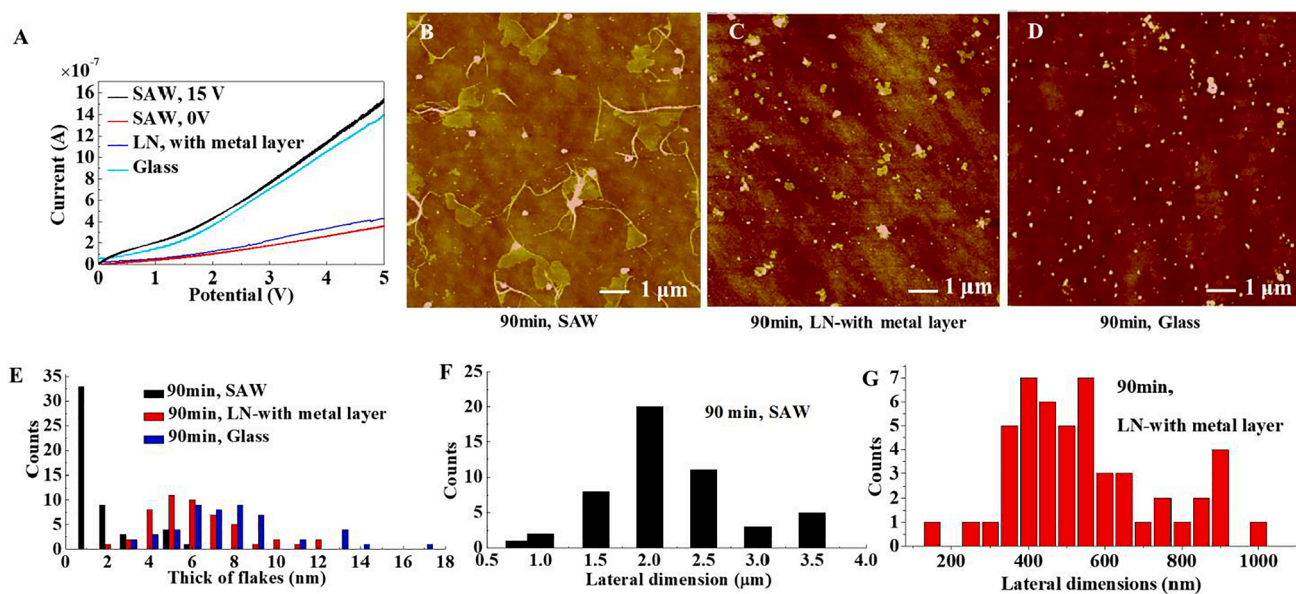

Fig. 5. Comparison of nanosheets data with different chips. (A) $I - V$ curves for MeOH/n-propanol mixture liquid measured using a two-wire probe station. The current flow was monitored through a voltage sweep from 0 to 5 V, under SAW excitation, LN substrate with metal layer chip and glass substrate chip. The AFM pictures of (B) SAW chip, (C) LN substrate with metal layer chip and (D) glass substrate chip. (E) Thickness distribution histograms of $Zn_2(bim)_4$ flakes (90 min) under SAW chip (black), LN substrate with metal layer chip (red), and glass substrate chip (blue). (F) Nanoflakes lateral dimension histograms under SAW chip for 90 min. (G) Nanoflakes lateral dimension histograms under LN substrate with metal layer chip for 90 min.

platform is applied with ultra-high voltages [46]. On the LN substrate chip with a metal layer, the *I-V* curve (Fig. 5A) under the voltage of 15 V is similar to that without using the SAW (SAW, 0 V), which means that no electric field was generated in the liquid with the addition of this metal layer. By applying an external voltage to the IDTs which on the glass substrate, the current generated in the solution is same with that under the agitation of the SAWs (with a voltage of 15 V). The obtained AFM images of the exfoliated MOFs after 90 min from these chips are shown in Fig. 5B-5D. From these figures, the largest dimension size of the nanosheet is obtained under the combined effect of acoustic and

electric fields, and then the smallest transverse size of the nanosheet is obtained under the electric field only.

Under the effect of acoustic field only (e.g., the LN chip with a metal layer), the average thickness of the nanosheet obtained is ~ 6 nm (with the red color in Fig. 5E). They are much thicker than the nanosheets (in black color) obtained under the agitation of both acoustic and electrical fields (Fig. 5E). Fig. 5F shows the lateral dimension of the nanosheets using the SAW agitation, with dimensions up to 3.5 μm and an average size of 2 μm. In contrast, on the LN substrate chip with only a metal layer (e.g., only electrical field effect), the lateral dimensions of the
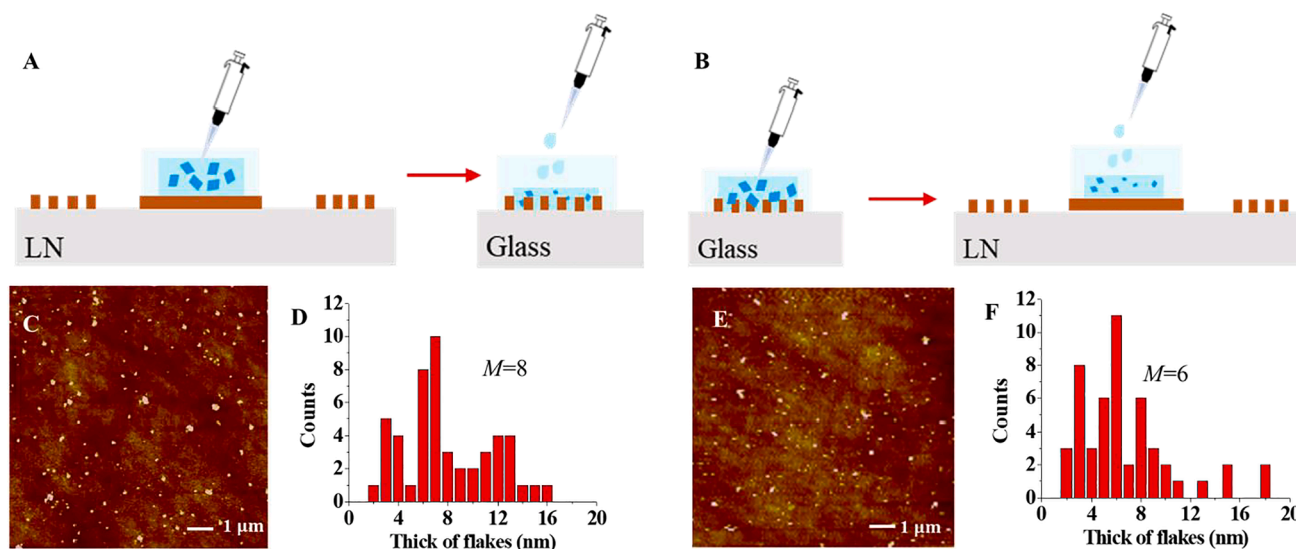
Fig. 6. Schematic illustration of two different methods, and thickness images obtained by AFM and thickness distribution histograms of the exfoliated $Zn_2(bim)_4$ nanoflakes. (A) Schematic illustration of method 1, (C) AFM images and (D) thickness distribution histograms of the exfoliated $Zn_2(bim)_4$ nanoflakes using the first method (i.e., acoustic field for 90 min, then electric field for 90 min). (B) Schematic illustration of method 2, (E) AFM images and (F) thickness distribution histograms of the exfoliated $Zn_2(bim)_4$ nanoflakes using the second method (i.e., electric field 90 min, then acoustic field for 90 min) M represents the median thickness.

nanosheets are much smaller, with an average size of 540 nm as shown in Fig. 5G.

The above results clearly show that the electric field plays an import role in the exfoliation process and can be applied to achieve 2D nanosheets with large cross-sectional area and ultrathin thickness. Under the action of electric field, the solution is ionized, and the insertion of H^+ ions into the layers of 3D MOF significantly expands the distance between the layers and weakens the interlayer bonding strength. This will promote the separation of different layers and also the subsequent release of the 2D flakes into the solution[35,36,47]. Whereas on the glass substrate with only the electric effect (without acoustic field), the average thickness of $Zn_2(bim)_4$ nanosheets is ~ 8 nm (as shown in blue color of Fig. 5E). Its lateral dimension is less than 200 nm which can be seem from the AFM picture shown in Fig. 5D. The above results confirm that the applied electric field can promote the fast exfoliation of the bulk MOF, but the size of the obtained nanosheets is small, without any single layer nanosheet generated.

In addition, to further understand the mechanism that underpins the acoustic field and electricity field exfoliation process, we have applied two different methods for exfoliation of the MOF nanosheets $(Zn_2(bim)_4)$. The first method we used to exfoliate the $Zn_2(bim)_4$ is under the acoustic fields for 90 min (using the LN chip with a metal layer), and then applied with the electric field (using the glass chip) for another 90 min. A schematic diagram of this method is shown in Fig. 6A. The second method is to apply the electric field (using the glass chip) for 90 min, and then apply the acoustic field using the LN chip with a metal layer) for another 90 min, as shown in Fig. 6B.

Fig. 6C to 6F show the AFM images and thickness distribution histograms of the samples obtained from these two methods. For the sample prepared using the first method, the average thickness of the nanosheets obtained is 8 nm and the lateral size is less than 200 nm, as shown in Fig. 6D. After 90 min of acoustic field action, followed by the electric field exfoliating for 90 min, the nanosheets (Fig. 5C) are mostly fractured laterally due to the intercalation of H^+ ions. The thickness of these 2D MOFs hardly thins further. Whereas for the sample prepared using the second method, we obtained 6 nm thick nanosheets with lateral dimension less than 200 nm as shown in Fig. 6F. This is because the size of the nanosheets (Fig. 5D) obtained by applying only the electric field is so small that the acoustic waves cannot continue to peel them effectively. Clearly, the results of nanosheets obtained from these two

methods are similar, while they are both much worse than those achieved by using a standard SAW device. The results shown in Fig. 3E clearly demonstrate that the combination of acoustic and electric fields can effectively promote the formation of single-layer MOFs.

4. Conclusions

A SAW device on a LN substrate is used in this paper to apply both acoustic field and electric field to effectively exfoliate bulk MOF-$Zn_2(bim)_4$ into monolayer-enriched 2D $Zn_2(bim)_4$. The thickness of the $Zn_2(bim)_4$ can be modulated by changing the exposure time of SAW. When the SAW exposure time is 20 min, the average thickness can reach to 5 nm. With the continuous increased of the exposure time to 90 min, ~66% of monolayers $Zn_2(bim)_4$ and the maximum lateral dimension up to ~ 3.5 μm have been achieved. We have investigated the effects of both acoustic field and electric field effects for exfoliation process. By shielding the accompanying electric field and using only acoustic waves induced by SAW, the obtained nanosheets are thicker and have smaller transverse dimensions. When only the electric field or only the acoustic wave field is applied to exfoliate bulk MOF-$Zn_2(bim)_4$, nanosheets with an average thickness of 6 or 8 nm and a small transverse dimension are obtained. By combining these two effects of acoustic and electric fields simultaneously (e.g., using SAWs), much better exfoliation results are obtained with a high percentage of monolayers and in the micron range dimensional size.

Declaration of Competing Interest

The authors declare that they have no known competing financial interests or personal relationships that could have appeared to influence the work reported in this paper.

Appendix A. Supplementary data

Supplementary data to this article can be found online at https://doi.org/10.1016/j.ultsonch.2022.105943.

REFERENCES

[1] K.S. Novoselov, A.K. Geim, S.V. Morozov, D. Jiang, Y. Zhang, S.V. Dubonos, I.V. Grigorieva, A.A. Firsov, Electric Field Effect in Atomically Thin Carbon Films, Science 306 (5696) (2004) 666–669.

[2] Y. Cao, V. Fatemi, S. Fang, K. Watanabe, T. Taniguchi, E. Kaxiras, P. Jarillo-Herrero, Unconventional superconductivity in magic-angle graphene superlattices, Nature 556 (7699) (2018) 43–50.

[3] B. Yang, J. Yin, Y.u. Chen, S. Pan, H. Yao, Y. Gao, J. Shi, 2D-Black-Phosphorus-Reinforced 3D-Printed Scaffolds: A Stepwise Countermeasure for Osteosarcoma, Adv Mater 30 (10) (2018) 1705611, https://doi.org/10.1002/adma.v30.1010.1002/adma.201705611.

[4] L. Sun, Y. Ying, H. Huang, Z. Song, Y. Mao, Z. Xu, X. Peng, Hubiao Huang, Zhigong Song, Yiyin Mao, Zhiping Xu, and Xinsheng Peng, *Ultrafast Molecule Separation through Layered WS2 Nanosheet Membranes*, Acs Nano 8 (6) (2014) 6304–6311.

[5] A.E. Ghazaly, H. Ahmed, A.R. Rezk, J. Halim, P.O.Å. Persson, L.Y. Yeo, J. Rosen, Ultrafast, One-Step, Salt-Solution-Based Acoustic Synthesis of Ti3C2 MXene, ACS Nano 15 (3) (2021) 4287–4293.

[6] M. Jian, R. Qiu, Y. Xia, J. Lu, Y.u. Chen, Q. Gu, R. Liu, C. Hu, J. Qu, H. Wang, X. Zhang, *Ultrathin water-stable metal-organic framework membranes for ion separation*. Science, Advances 6 (23) (2020), https://doi.org/10.1126/sciadv.aay3998.

[7] H. Zhang, Ultrathin Two-Dimensional Nanomaterials, ACS nano 9 (10) (2015) 9451–9469.

[8] Y.K. Jo, M. Kim, X. Jin, I.Y. Kim, J. Lim, N.-S. Lee, Y.K. Hwang, J.-S. Chang, H. Kim, S.-J. Hwang, Hybridization of a Metal-Organic Framework with a Two-Dimensional Metal Oxide Nanosheet: Optimization of Functionality and Stability, Chemistry of Materials 29 (3) (2017) 1028–1035.

[9] W. Lu, Z. Wei, Z.-Y. Gu, T.-F. Liu, J. Park, J. Park, J. Tian, M. Zhang, Q. Zhang, T. Gentle III, M. Bosch, H.-C. Zhou, Tuning the structure and function of metal-organic frameworks via linker design, Chem Soc Rev 43 (16) (2014) 5561–5593.

[10] H. Chen, Q. Qiu, S. Sharif, S. Ying, Y. Wang, Y. Ying, Solution-Phase Synthesis of Platinum Nanoparticle-Decorated Metal-Organic Framework Hybrid Nanomaterials as Biomimetic Nanoenzymes for Biosensing Applications, ACS Appl Mater Interfaces 10 (28) (2018) 24108–24115.

[11] Q. Qiu, H. Chen, S. Sharif, Z. You, S. Ying, Y. Wang, Y. Ying, Ultrathin noble metal nanoplates decorated metal-organic framework nanosheets as 2D/2D heterojunction nanobionic catalysts for explosive residues monitoring, 2D Materials 6 (3) (2019) 035008, https://doi.org/10.1088/2053-1583/ab1165.

[12] M.-S. Yao, X.-J. Lv, Z.-H. Fu, W.-H. Li, W.-H. Deng, G.-D. Wu, G. Xu, Layer-by-Layer Assembled Conductive Metal-Organic Framework Nanofilms for Room-Temperature Chemiresistive Sensing, Angew Chem Int Ed Engl 56 (52) (2017) 16510–16514.

[13] D. Xu, D. Chao, H. Wang, Y. Gong, R. Wang, B. He, X. Hu, H.J. Fan, Flexible Quasi-Solid-State Sodium-Ion Capacitors Developed Using 2D Metal-Organic-Framework Array as Reactor, Advanced Energy Materials 8 (13) (2018) 1702769, https://doi.org/10.1002/aenm.v8.1310.1002/aenm.201702769.

[14] K. Rui, G. Zhao, Y. Chen, Y. Lin, Q. Zhou, J. Chen, J. Zhu, W. Sun, W. Huang, S.X. Dou, Hybrid 2D Dual-Metal–Organic Frameworks for Enhanced Water Oxidation Catalysis, Advanced Functional Materials 28 (26) (2018) 1801554, https://doi.org/10.1002/adfm.v28.2610.1002/adfm.201801554.

[15] X. Wang, et al., Reversed thermo-switchable molecular sieving membranes composed of two-dimensional metal-organic nanosheets for gas separation, Nat Commun 8 (2017) 14460.

[16] F. Cao, M. Zhao, Y. Yu, B.o. Chen, Y. Huang, J. Yang, X. Cao, Q. Lu, X. Zhang, Z. Zhang, C. Tan, H. Zhang, Synthesis of Two-Dimensional CoS1.097/Nitrogen-Doped Carbon Nanocomposites Using Metal-Organic Framework Nanosheets as Precursors for Supercapacitor Application, J Am Chem Soc 138 (22) (2016) 6924–6927.

[17] T. Bauer, Z. Zheng, A. Renn, R. Enning, A. Stemmer, J. Sakamoto, A.D. Schlüter, Synthesis of free-standing, monolayered organometallic sheets at the air/water interface, Angew Chem Int Ed Engl 50 (34) (2011) 7879–7884.

[18] T. Kambe, R. Sakamoto, K. Hoshiko, K. Takada, M. Miyachi, J.-H. Ryu, S. Sasaki, J. Kim, K. Nakazato, M. Takata, H. Nishihara, π-Conjugated nickel bis(dithiolene) complex nanosheet, J Am Chem Soc 135 (7) (2013) 2462–2465.

[19] K. Zhao, S. Liu, G. Ye, Q. Gan, Z. Zhou, Z. He, High-yield bottom-up synthesis of 2D metal–organic frameworks and their derived ultrathin carbon nanosheets for energy storage, Journal of Materials Chemistry A 6 (5) (2018) 2166–2175.

[20] M. Zhao, Y. Wang, Q. Ma, Y. Huang, X. Zhang, J. Ping, Z. Zhang, Q. Lu, Y. Yu, H. Xu, Y. Zhao, H. Zhang, Ultrathin 2D Metal-Organic Framework Nanosheets, Adv Mater 27 (45) (2015) 7372–7378.

[21] Y. Wang, M. Zhao, J. Ping, B.o. Chen, X. Cao, Y. Huang, C. Tan, Q. Ma, S. Wu, Y. Yu, Q. Lu, J. Chen, W. Zhao, Y. Ying, H. Zhang, Bioinspired Design of Ultrathin 2D Bimetallic Metal-Organic-Framework Nanosheets Used as Biomimetic Enzymes, Adv Mater 28 (21) (2016) 4149–4155.

[22] Y. Yang, K. Goh, R. Wang, T.-H. Bae, High-performance nanocomposite membranes realized by efficient molecular sieving with CuBDC nanosheets, Chem Commun (Camb) 53 (30) (2017) 4254–4257.

[23] M.J. Cliffe, E. Castillo-Martínez, Y. Wu, J. Lee, A.C. Forse, F.C.N. Firth, P.Z. Moghadam, D. Fairen-Jimenez, M.W. Gaultois, J.A. Hill, O.V. Magdysyuk, B. Slater, A.L. Goodwin, C.P. Grey, Metal-Organic Nanosheets Formed via Defect-Mediated Transformation of a Hafnium Metal-Organic Framework, J Am Chem Soc 139 (15) (2017) 5397–5404.

[24] P. Chandrasekhar, A. Mukhopadhyay, G. Savitha, J.N. Moorthy, Orthogonal self-assembly of a trigonal triptycene triacid: signaling of exfoliation of porous 2D metal–organic layers by fluorescence and selective CO2 capture by the hydrogen-bonded MOF, Journal of Materials Chemistry A 5 (11) (2017) 5402–5412.

[25] Y. Peng, Y. Li, Y. Ban, H. Jin, W. Jiao, X. Liu, W. Yang, Metal-organic framework nanosheets as building blocks for molecular sieving membranes, Science 346 (6215) (2014) 1356–1359.

[26] Q. Qiu, H. Chen, Z. You, Y. Feng, X. Wang, Y. Wang, Y. Ying, Shear Exfoliated Metal-Organic Framework Nanosheet-Enabled Flexible Sensor for Real-Time Monitoring of Superoxide Anion, ACS Appl Mater Interfaces 12 (5) (2020) 5429–5436.

[27] Y. Ding, Y.-P. Chen, X. Zhang, L. Chen, Z. Dong, H.-L. Jiang, H. Xu, H.-C. Zhou, Controlled Intercalation and Chemical Exfoliation of Layered Metal-Organic Frameworks Using a Chemically Labile Intercalating Agent, J Am Chem Soc 139 (27) (2017) 9136–9139.

[28] H.-L. Liu, Y.-J. Chang, T. Fan, Z.-Y. Gu, Two-dimensional metal-organic framework nanosheets as a matrix for laser desorption/ionization of small molecules and monitoring enzymatic reactions at high salt concentrations, Chem Commun (Camb) 52 (88) (2016) 12984–12987.

[29] S. Leubner, V.E.G. Bengtsson, K. Synnatschke, J. Gosch, A. Koch, H. Reinsch, H. Xu, C. Backes, X. Zou, N. Stock, Synthesis and Exfoliation of a New Layered Mesoporous Zr-MOF Comprising Hexa- and Dodecanuclear Clusters as Well as a Small Organic Linker Molecule, J Am Chem Soc 142 (37) (2020) 15995–16000.

[30] T. Zheng, C. Wang, C. Xu, Tritoroidal particle rings formation in open microfluidics induced by standing surface acoustic waves, Electrophoresis 41 (10-11) (2020) 983–990.

[31] T. Zheng, Y. Liu, C. Xu, H. Lu, C. Wang, Focusing surface acoustic waves assisted electrochemical detector in microfluidics, Electrophoresis 41 (10-11) (2020) 860–866.

[32] M.d. Mohiuddin, Y. Wang, A. Zavabeti, N. Syed, R.S. Datta, H. Ahmed, T. Daeneke, S.P. Russo, A.R. Rezk, L.Y. Yeo, K. Kalantar-Zadeh, Liquid Phase Acoustic Wave Exfoliation of Layered MoS2: Critical Impact of Electric Field in Efficiency, Chemistry of Materials 30 (16) (2018) 5593–5601.

[33] S. Marqus, H. Ahmed, M. Ahmed, C. Xu, A.R. Rezk, L.Y. Yeo, Increasing Exfoliation Yield in the Synthesis of MoS2 Quantum Dots for Optoelectronic and Other Applications through a Continuous Multicycle Acoustomicrofluidic Approach, ACS Applied Nano Materials 1 (6) (2018) 2503–2508.

[34] Y.Q. Fu, J.K. Luo, N.T. Nguyen, A.J. Walton, A.J. Flewitt, X.T. Zu, Y. Li, G. McHale, A. Matthews, E. Iborra, H. Du, W.I. Milne, Advances in piezoelectric thin films for acoustic biosensors, acoustofluidics and lab-on-chip applications, Progress in Materials Science 89 (2017) 31–91.

[35] Y. Yang, H. Hou, G. Zou, W. Shi, H. Shuai, J. Li, X. Ji, Electrochemical exfoliation of graphene-like two-dimensional nanomaterials, Nanoscale 11 (1) (2019) 16–33.

[36] Y. Fang, X. Li, J. Li, C. Yao, H.Y. Hoh, X. Hai, J. Lu, C. Su, Janus electrochemical exfoliation of two-dimensional materials, Journal of Materials Chemistry A 7 (45) (2019) 25691–25711.

[37] T. Li, et al., A novel water-stable two-dimensional zeolitic imidazolate frameworks thin-film composite membrane for enhancements in water permeability and nanofiltration performance, Chemosphere 261 (2020), 127717.

[38] H.-J. Xu, Y.-X. Liu, Z. Shen, Y.-Q. Tian, X.-Z. You, {[Zn2(Bim)3(OH)(H2O)]·(DMF)(H2O)3}∞: a Two Dimensional Coordination Polymer with Layer Silicate-like Structure, Zeitschrift für anorganische und allgemeine Chemie 631 (8) (2005) 1349–1351.

[39] T.M. Nenoff, Hydrogen purification: MOF membranes put to the test, Nat Chem 7 (5) (2015) 377–378.

[40] T. Zheng, C. Wang, Q. Hu, S. Wei, The role of electric field in microfluidic heating induced by standing surface acoustic waves, Applied Physics Letters 112 (23) (2018) 233702, https://doi.org/10.1063/1.5030052.

[41] T. Zheng, C. Wang, C. Xu, Q. Hu, S. Wei, Patterning microparticles into a two-dimensional pattern using one column standing surface acoustic waves, Sensors and Actuators A: Physical 284 (2018) 168–171.

[42] J. Wang, X. Wang, L.i. Wan, Y. Yang, S. Wang, An Effective Method for Bulk Obtaining Graphene Oxide Solids, Chinese Journal of Chemistry 28 (10) (2010) 1935–1940.

[43] Y. Peng, Y. Li, Y. Ban, W. Yang, Two-Dimensional Metal-Organic Framework Nanosheets for Membrane-Based Gas Separation, Angew Chem Int Ed Engl 56 (33) (2017) 9757–9761.

[44] B. Liu, X. Wang, H. Liu, Y. Zhai, L. Li, H. Wen, 2D MOF with electrochemical exfoliated graphene for nonenzymatic glucose sensing: Central metal sites and oxidation potentials, Anal Chim Acta 1122 (2020) 9–19.

[45] Z. Yu, J. Peng, Y. Liu, W. Liu, H. Liu, Y. Guo, Amine-assisted exfoliation and electrical conductivity modulation toward few-layer FePS3 nanosheets for efficient hydrogen evolution, Journal of Materials Chemistry A 7 (23) (2019) 13928–13934.

[46] A.R. Rezk, H. Ahmed, T.L. Brain, J.O. Castro, M.K. Tan, J. Langley, N. Cox, J. Mondal, W.u. Li, M. Ashokkumar, L.Y. Yeo, Free Radical Generation from High-Frequency Electromechanical Dissociation of Pure Water, Physical Chemistry Letter 11 (12) (2020) 4655–4661.

[47] Z. Zeng, Z. Yin, X. Huang, H. Li, Q. He, G. Lu, F. Boey, H. Zhang, Single-layer semiconducting nanosheets: high-yield preparation and device fabrication, Angew Chem Int Ed Engl 50 (47) (2011) 11093–11097.